Coupled Systems Mechanics, *Vol. 7, No. 4 (2018) 407-420*
DOI: https://doi.org/10.12989/csm.2018.7.4.407

Hydrodynamic coupling distance between a falling sphere and downstream wall

Cheng-Chuan Lin*, Hung-Tien Huang[a] and Fu-Ling Yang[b]

Department of Mechanical Engineering, National Taiwan University,
No. 1, Sec. 4, Roosevelt Rd., Taipei 10617, Taiwan (R.O.C.)

(Received January 29, 2018, Revised January 30, 2018, Accepted January 31, 2018)

Abstract. In solid-liquid two phase flow, the knowledge of how descending solid particles affected by the presence of downstream wall is important. This work studies at what interstitial distance the velocity of a vertically descending sphere is affected by a downstream wall as a consequence of wall-modified hydrodynamic forces through a validated dynamic model. This interstitial distance-the hydrodynamic coupling distance δ_c-is found to decay monotonically with the approach Stokes number *St* which compares the particle inertia to viscous drag characterized by the quasi-steady Stokes' drag. The scaling relation δ_c-*St*-1 decays monotonically as literature below the value of *St* equal to 10. However, the faster diminishing rate is found above the threshold value from *St*=10-40. Furthermore, an empirical relation of δ_c-*St* shows dependence on the drop height which clearly indicates the non-negligible effect of unsteady hydrodynamic force components, namely the added mass force and the history force. Finally, we attempt a fitting relation which embedded the particle acceleration effect in the dependence of fitting constants on the diameter-scaled drop height.

Keywords: hydrodynamic coupling; Stokes number; wall effect; added mass force; history force

1. Introduction

Particle-laden solid-liquid two-phase flows appear in a wide range of industrial applications (fluidized bed, slurry transport, pharmaceutical process, suspension filtering) and natural events (debris flows, sedimentation, soil liquefaction). Though we have established fair knowledge to describe the motion of a continuum fluid and its transport phenomenon, the addition of a second phase in discrete form brings new mechanisms for bulk momentum and energy transport. For example, when particles possess sufficient inertia to move relative to local fluid motion, they can interact with local flow structure and even come into contact, collide and rebound to redistribute bulk momentum and energy. Hence, the dynamic process at the constituent size level shall characterize the microscopic mechanisms for bulk macroscopic transport process. Extensive works

*Corresponding author, Ph.D. Student, E-mail: f00522316@ntu.edu.tw
[a]M.Sc., E-mail: r03522123@ntu.edu.tw
[b]Professor, E-mail: fulingyang@ntu.edu.tw

http://www.techno-press.org/?journal=csm&subpage=8 ISSN: 2234-2184 (Print), 2234-2192 (Online)

have been reported for how the particle-wall and particle-particle collision process is modified by interstitial liquid in terms of a wet coefficient of restitution, e_{wet}, as the ratio of rebound velocity to that of the impact. Hence, e_{wet} measures the loss proportion of particle kinetic energy lost to viscous dissipation as well as inelastic deformation. Various empirical evidences have shown that e_{wet} diminishes monotonically from the dry coefficient of restitution with a dimensionless particle Stokes number, $St_i=m_pU_i/6\pi\mu a^2$, that compares particle inertia force to hydrodynamic drag characterized by Stokes drag (Joseph 2001, Gondret *et al.* 2002, Yang and Hunt 2006, Simeonov 2015). Here, m_p is the mass of the solid particle of a characteristic radius a and solid density ρ_s, U_i is particle impact velocity, and μ is liquid viscosity. For a spherical particle, $m_p=4/3\pi a^3\rho_s$ and it is common to express $St_i=(\rho_s/\rho)Re_i/9$ in terms of the solid-to-fluid density ratio, $\gamma=\rho_s/\rho$, and an impact Reynolds number, $Re_i=2a\rho U_i/\mu$.

Other than direct collisions, it has been reported that the motion of two non-touching immersed solid objects may affect each other through the interstitial liquid. Joseph *et al.* (2001) conducted systematic experiments to measure the velocity of an immersed spherical pendulum when it swung towards a vertical flat surface at the pendulum lowest trajectory. Another set of control experiments was conducted by removing the target wall while using the same pendulum set up and experimental fluid. The velocity-trajectory profiles from the two sets of experiments were compared as shown in Fig. 1(a) and pendulum velocity deduction was detected when it moved close enough to the wall. Joseph *et al.* (2001) call this interstitial gap at which the wall has a modifying effect on local hydrodynamic force as the critical distance of wall influence, δ_c, though no clear definition has been given. This length scale is then linked to the particle approach Stokes number, St, calculated using the instantaneous approach velocity when the sphere moved to 1.5 diameters from the wall. As we no longer use the particle impact velocity to calculate particle Stokes number, the subscript 'i' has been removed for distinction. A monotonic decay of δ_c with St was reported over the range of $0\leq\delta_c\leq a$ and $9\leq St\leq 68$ which phenomenon is later discussed by Izard *et al.* (2014) for how to set the initial condition of an immersed collision model.

Limiting to the condition when the sphere approached at a constant velocity, Izard *et al.* (2014) consider the lubrication force as the primary hydrodynamic force in which the wall amplifies the Stokes' drag by the inverse of radius-scaled interstitial gap, denoted by $\delta^*=\delta/a$. A scaling is given on the particle motion as $m_p du/dt\sim 6\pi\mu a u/\delta^*$ which is further reduced to a dimensionless form $St\, du^*/dt^*\sim u^*/\delta^*$ using the approach velocity and the sphere radius a in the scaling analysis (Davis *et al.* 1986, Joseph *et al.* 2001). Based on this, the authors propose a scaling for the critical distance as $\delta_c^*\sim St^{-1}$ and claimed agreement to the experimental data by Joseph *et al.* (2001) as shown in Fig. 1(b). Though the monotonic decay of δ_c^* with St is captured with this scaling argument, it may be argued that the experimentally measured δ_c^* seems to decay slower than St^{-1} below St~30-40 but faster above this St.

Hence, this work is set to further examine this phenomenon with a validated dynamic model developed by Yang (2006, 2010). As the pendulum velocity reduction near wall may be interpreted as a non-contact coupling of the sphere dynamics to the wall through the action of ambient fluid, we prefer to call this phenomenon as hydrodynamic coupling (Yang 2006). A clear definition will be introduced to define the hydrodynamic coupling distance based on the approach velocity following the original concept of Joseph *et al.* (2001). As the pendulum swing examined by Joseph *et al.* (2001) is always unsteady unlike the steady approach assumed by Izard *et al.* (2014), we decide to study the vertical descent of a sphere towards a wall as both steady and transient dynamics can be developed. The knowledge of hydrodynamic coupling distance provides

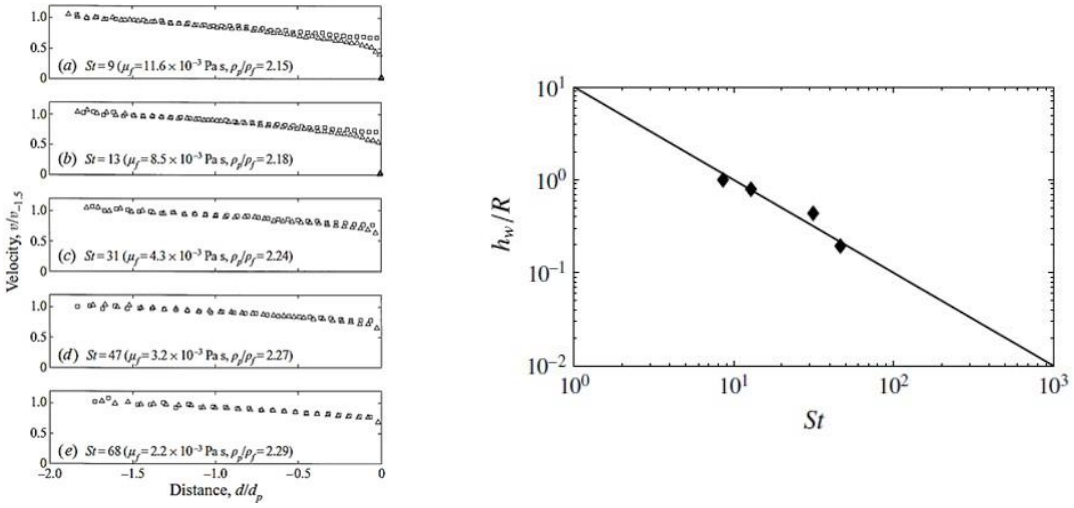

Fig. 1(a) Experimental evidence showing how a downstream wall at d=0 modifies the pendulum approach velocity. The comparison is made for the velocity-position data for a free swing pendulum (square) and one moving towards a wall (triangle), copied from Fig. 9 in Joseph *et al.* (2001). (b) Coupling distance (h_w here scaled by the sphere radius R) as a function of approach Stokes number. Comparison of the data from Fig. 1(a) and the scaling argument by Izard *et al.* (2014), copied from Fig. 11 in Izard *et al.* (2014)

crucial information for the modeling and simulation of both immersed collision process as it can be used to determine the minimum computation domain (Hou *et al.* 2012, Kempe and Fröhlich 2012, Li *et al.* 2011, Wang and Eldredge 2015). The information also complements the existing theories of fluid-structure interaction problems as it gives a physical and explicit criterion to determine if the existing theories and computation algorithms developed under the infinite fluid domain assumption remains valid (Tallec and Mouro 2001, Soares 2012, Ibrahimbegovic *et al.* 2016, Lefrançois *et al.* 2016). In the following, we introduce the dynamic model and how we solve and process the numerical data to obtain the desired information and then conclude the work with discussions and possible future investigations.

2. Dynamic model

Consider a solid sphere of radius a and density ρ_s that descends towards a horizontal wall from an interstitial distance δ at velocity U in an incompressible and viscous liquid of density ρ and viscosity μ as sketched in Fig. 2. To describe this motion, Yang (2010) has proposed a model based on an experimentally-validated model developed for the immersed pendulum swing examined by Joseph *et al.* (Yang 2006). The model is composed of a sphere trajectory equation and an equation of motion as

$$\begin{cases} \dfrac{d\delta}{dt} = -U \\ m_p \dfrac{dU}{dt} = (m_p - m_f)g + F_{QD}(Re, \delta^*) + F_{AM}(\delta^*) + F_H(Re, \delta^*) \end{cases} \quad (1a, b)$$

In Eq. (1b), $m_f = (4\pi/3)a^3\rho$ is the fluid mass displaced by the sphere volume so that the first term on the right hand side of Eq. (1b) is the effective gravity force taking into account of buoyancy force. The following terms are the quasi-steady viscous drag, $F_{QD}(Re, \delta^*)$, and two unsteady components-the added mass force, $F_{AM}(\delta^*)$, and the history force $F_H(Re, \delta^*)$-as the squeeze flow is intrinsically unsteady. The quasi-steady viscous drag is expressed as the Stokes drag multiplied with a correction factor C as

$$F_{QD}(Re, \delta^*) = -6\pi\mu a U C(Re, \delta^*). \tag{2}$$

When the sphere is far away from the wall and moves at moderate particle Reynolds number Re<800 calculated by a local velocity $U(\delta^*)$, $C(Re, \delta^*)=1+0.15Re^{0.687}$ which corrects Stokes' drag for liquid inertia (Clift, Grace and Weber 1978). When the sphere moves to the vicinity of wall, this correction factor is changed to the analytic *wall correction factor* by Cox and Brenner (1967) as

$$C(\delta^*, Re) = \frac{1}{\delta^*}\left[1 - \frac{1}{5}\left(1 + \frac{1}{4}Re\right)\delta^* log\delta^*\right], \tag{3}$$

when the far-field factor falls below this near-field factor. This factor is derived analytically by solving the unsteady Stokes equation for fluid motion between the moving sphere and the wall taking into account of liquid inertial with the asymptotic analysis. This wall correction factor grows monotonically with diminishing δ^* and asymptotes to the lubrication force when δ^* approaches zero, leaving only the first term of Eq. (3) that recovers the argument by Izard *et al.* (2014).

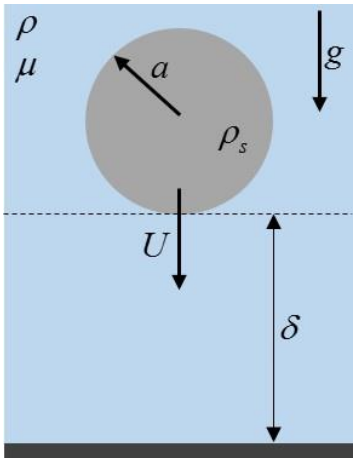

Fig. 2 Illustration of the studied problem that a fully immersed sphere in vertical descent towards a downstream wall

The added mass force can be developed by the potential flow theory in which the flow around the approaching solid sphere is constructed by superposing infinitely many image dipoles of specific strengths and at specific locations to satisfy the no-penetration boundary condition on both solid surfaces (Yang 2010) as

$$F_{AM}(\delta^*) = -\frac{1}{2} m_f \left[1 + W(\delta^*)\right] \frac{dU}{dt} + \frac{1}{4} \frac{m_f}{a} U^2 \frac{dW(\delta^*)}{d\delta^*}, \tag{4}$$

where $W(\delta^*)$ is a wall function of δ^* as

$$W(\delta^*) = \sum_{N=1}^{\infty} 3\left(\frac{\alpha^* - \beta^*}{\alpha^{*N+1} - \beta^{*N+1}} \right)^3 = \sum_{N=1}^{\infty} \varpi(\delta^*), \tag{5}$$

with $\alpha^* = (\delta^* + 1) + \sqrt{(\delta^* + 1)^2 - 1}$ and $\beta^* = (\delta^* + 1) - \sqrt{(\delta^* + 1)^2 - 1}$. The first term on the right hand side of Eq. (4) is similar to the classic added mass force in the aspect of its dependence on the sphere acceleration, dU/dt, and some apparent fluid mass, augmented here by $W(\delta^*)$ due to the infinitely many images. Once the sphere moves closer to the wall, the strength and the location of these image dipoles change accordingly to induce variation in the total fluid impulse that in turn renders the last term of Eq. (4) involving with $dW/d\delta^*$. This component may be interpreted as a dynamic pressure force as if we multiply a component ρU^2 with a surface projection area πa^2.

For application, a simpler formula for $W(\delta^*)$ is necessary and Yang has proposed a composite formula by integrating a far-field five-term partial sum $W_5(\delta^*)$ and a near-field Padé approximation, $P_{54}(\delta^*)$, with a bridge function, $B(\delta^*)$, as

$$W(\delta^*) = \begin{cases} W_5(\delta^*) = \sum_{N=1}^{5} \varpi(\delta^*) & \text{for } \delta^* \geq 0.1287 \\ B(\delta^*) = \sum_{j=0}^{3} a_j \left(\delta^* + 1\right)^j & \text{for } 0.0618 \leq \delta^* \leq 0.1287 \\ P_{56}(\delta^*) = \dfrac{\sum_{j=0}^{5} b_j \left(\delta^* + 1\right)^j}{\sum_{j=0}^{6} c_j \left(\delta^* + 1\right)^j} & \text{for } \delta^* \leq 0.0618 \end{cases} \tag{6}$$

with the expansion coefficients summarized in Table 1. This was developed to ensure that the deviation from the 200-term partial sum of Eq. (5) is below 0.4% for all $\delta^* \geq 0$ and this particular 200-term partial sum deviates from the analytic limiting value at $\delta^* = 0$ by at most 0.61%. Hence, an overall convergence to the infinite series can be confirmed.

Table 1 Expansion coefficient for the composite formula for $W(\delta^*)$ in Eq. (6).

	j=0	1	2	3	4	5	6
a_j	44.27	-110.95	94.04	-26.80			
b_j	0.605605	984.634	5.835E5	1.513E8	1.606E10	4.743E11	
c_j	1	1642.3	9.868E5	2.621E8	2.292E10	1.027E12	5.112E12

The differentiation of $W(\delta^*)$ with respect to δ^* can be evaluated with term-by-term differentiation and a three-term partial sum is used as a far-field approximation when $\delta^* > 1$ (Yang 2006). However, the slow convergence of the entry derivatives $d\varpi/d\delta^*$ makes the partial sum

approximation unpractical in the near field while the unique structure of the continued fraction in $\varpi(\delta^*)$ is destroyed upon differentiation and hence $dW/d\delta^* \neq dP_{54}/d\delta^*$. Hence, a least-square fitting formula, with a standard deviation of 9.24×10^{-4}, is sought for the 40-term partial sum to complete the final composite formula for $\delta^* \leq 1$, using $h^*=\delta^*+1$ for a more compact expression, as

$$\frac{dW}{d\delta^*}=\begin{cases}\displaystyle\sum_{N=1}^{3}\frac{d\varpi}{d\delta^*}=\frac{1}{128h^{*2}\left(h^{*2}-1\right)\left(2h^{*2}-1\right)^3}-\frac{3h^*\left(4h^{*2}-3\right)}{2\left(h^{*2}-1\right)\left(4h^{*2}-1\right)^4}\\ \quad+\dfrac{h^*}{2\left(h^{*2}-1\right)\left(4h^{*2}-1\right)^3}-\dfrac{8h^{*4}-8h^{*2}+1}{128h^{*4}\left(h^{*2}-1\right)\left(2h^{*2}-1\right)^4}\\ \quad+\dfrac{1}{16h^{*2}\left(h^{*2}-1\right)}-\dfrac{2h^{*2}-1}{16h^{*4}\left(h^{*2}-1\right)} \quad \text{for } h^*=\delta^*+1>2\\ \displaystyle\sum_{N=1}^{40}\frac{d\varpi}{d\delta^*}=0.241-2.3\times10^{-4}\delta^{*-1/2}-0.311\delta^{*1/2}+6.6\times10^{-2}\delta^*\\ \quad+9.8\times10^{-2}log\left(\delta^*\right)-2.06\times10^{-4}log\left(\delta^*\right)\delta^{*-1/2} \quad \text{for } h^*\leq 2\end{cases} \tag{7}$$

The last history force $F_H(Re, \delta^*)$ accounts for the temporal delay in the boundary-layer development when the relative velocity between a solid surface and its adjacent fluid varies in time. Yang considered how a wall-augmented pressure field can result in a faster free stream tangential velocity at the sphere surface to propose

$$F_H(\delta^*,t,Re)=-6\pi\mu aH(\delta^*)^{3/2}\int_0^t\frac{dU}{d\tau}K(Re,t-\tau)d\tau, \tag{8}$$

with $H(\delta^*)=1+W(\delta^*)$ that can be computed according to Eq. (6). In Eq. (8), $K(Re, t-\tau)$ is a semi-empirical time kernel developed by Mei and Adrian (1992) for $Re<100$ as

$$K(t-\tau)=\left\{\left[\frac{\pi(t-\tau)\nu}{a^2}\right]^{1/4}+\left[\frac{\pi}{2}\frac{U^3(t-\tau)^2}{a\nu\left(0.75+0.105Re\right)^3}\right]^{1/2}\right\}^{-2}, \tag{9}$$

which follows Basset classic kernel $(t-\tau)^{-1/2}$ at shorter times but decays faster at large times.

The final equation of motion for a fully immersed solid sphere of mass m_p released from an initial drop height of H to descend vertically towards a wall can be formulated as

$$\begin{cases}\dfrac{d\delta}{dt}=-U\\ m_p\dfrac{dU}{dt}=F_G-F_B+F_D(Re,\delta^*)+F_{AM}(\delta^*)+F_H(Re,\delta^*)\end{cases} \tag{10a, b}$$

where a rectangular coordinate system is defined from the wall. The initial drop height gives $\delta(0)=H$ and zero initial velocity gives $d\delta/dt(0)=0$ which leads to $m_p dU/dt=F_G-F_B-1/2m_f[1+W(H/a)]dU/dt$ in Eq. (10b). This set of equations can be made dimensionless using the

sphere radius, a, and terminal velocity, U_T, as characteristic length and velocity scales into

$$\begin{cases} \dfrac{d\delta^*}{dt^*} = -u^* \\ \dfrac{\rho_P}{\rho}\dfrac{du^*}{dt^*} = \left(\dfrac{\rho_P}{\rho}-1\right)\dfrac{ag}{U_T^2} - \dfrac{1}{2}\left[1+W(\delta^*)\right]\dfrac{du^*}{dt^*} + \dfrac{1}{4}u^{*2}\dfrac{dW(\delta^*)}{d\delta^*} \\ \qquad -\dfrac{18}{Re_T}u^*C(Re,\delta^*) - \dfrac{18}{Re_T}H(\delta^*)^{3/2}\int_0^t \dfrac{du^*}{d\tau^*}K(Re,t^*-\tau^*)d\tau^* \end{cases} \tag{11a, b}$$

with $\delta^*=\delta/D$, $u^*=u/U_T$, and $t^*=2a/U_T$, and $Re_T=2a\rho U_T/\mu$. If we further divide out the solid-to-liquid density ratio $\gamma=\rho_p/\rho$, we may rewrite Eq. (11b) to reveal the dependence on particle Stokes number and density ratio as

$$\begin{aligned} \frac{du^*}{dt^*} &= \left(1-\frac{1}{\gamma}\right)\frac{ag}{U_T^2} - \frac{1}{2\gamma}\left[1+W(\delta^*)\right]\frac{du^*}{dt^*} + \frac{1}{4\gamma}\frac{dW(\delta^*)}{d\delta^*}u^{*2} \\ &\quad -\frac{2}{St}u^*C(Re,\delta^*) - \frac{2}{St}H(\delta^*)^{3/2}\int_0^t \frac{du^*}{d\tau^*}K(Re,t^*-\tau^*)d\tau^* \end{aligned} \tag{12}$$

Eq. (12) clearly demonstrates how particle inertial counteracts buoyancy force and F_{AM} through the factor $1/\gamma$ while the leading coefficient $1/St$ in the last two terms also indicates the diminishing effect of viscous force components by particle inertia. The set of equations Eq. (11a) and Eq. (12) were solved numerically by the fourth-order Runge-Kutta method.

To provide a reference descent dynamics without wall effect $U_\infty(t) = u^*_\infty(t)U_T$, we turned off all the wall correction factors while keeping identical fluid and sphere properties and initial conditions. For example, first solved the descent dynamics of the same sphere of density ρ_s=2532.4 kg/m^3 and diameter D=42 mm in four liquids of different viscosities μ=46.8, 75, 134.4 and 241.8 cP but identical liquid density ρ=1245 kg/m^3 to achieve four descents towards their terminal velocities Fig. 3. Though real liquid density should change with its viscosity, the degree of variation is much milder and hence we kept it a constant to fix the solid-to-liquid density ratio. It is checked that changing density accordingly does not change the results we observe for the coupling distance.

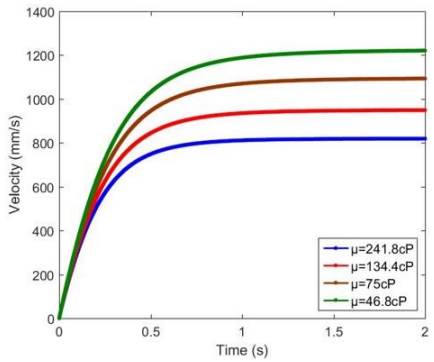

Fig. 3 The velocity profile towards a terminal velocity for a solid sphere of diameter D=42 mm and density ρ_s=2532.4 kg/m^3 descending in a fluid of different viscosities μ but identical density ρ=1245 kg/m^3

We then introduced a target wall at different distances, H, from the release point to simulate the descent dynamics, $U_H(t, \delta)$, and compare it to $U_\infty(t)$. We define the occurrence of hydrodynamic coupling by when $U_H(t, \delta)$ drops by 5%$U_\infty(t)$ and the associated interstitial distance as the hydrodynamic coupling distance. Two sets of comparison were examined.

In the first set of comparison, the wall was introduced far enough so that the sphere developed its terminal velocity U_T before experiencing the wall effect. For the four examined liquid viscosities, μ=46.8, 75, 134.4 and 241.8 cP, we chose H=65D, 55D, 45D and 40D, accordingly, which height was determined from the descent dynamics without wall $H = \int_0^T U_\infty(t)dt$ by choosing a moment T after $U_\infty(t)$ had reached U_T. A shorter distance is needed when descending in a more viscous fluid for its stronger viscous dissipation.

For example, H=40D was chosen to compute the descend dynamics of a sphere of diameter D=42 mm in a liquid of μ=241.8 cP and ρ=1245 kg/m^3 as shown in Fig. 4(a). The developed terminal velocity agrees to the theoretical value shown by the green dashed line and the sphere abrupt deceleration near wall was examined at a finer time resolution in Fig. 4(b). We find the sphere velocity dropped below 0.95U_T between t=2.260081 s and 2.260082 s with the corresponding velocity and gap data denoted by $(U_{H,+1}, \delta^*_{+1}a)$ and $(U_{H,-1}, \delta^*_{-1}a)$. The diameter-scaled coupling distance, δ^*_c, can then be interpolated by

$$\frac{0.95U_T - U_{H,-1}}{U_{H,+1} - U_{H,-1}} = \frac{\delta^*_c - \delta^*_-}{\delta^*_+ - \delta^*_-} \tag{13}$$

to obtain δ^*_c=1.047×10^{-2}. The associated particle approach Stokes number is evaluated with U_T to give St=38.33.

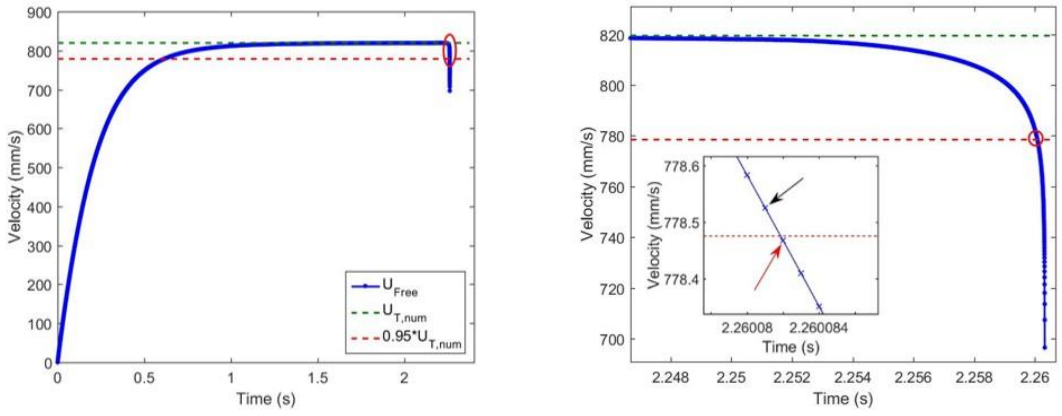

(a) (b)

Fig. 4(a) Comparison of the descending velocity profile of a solid sphere towards wall with the terminal velocity (green dashed line) and its 5% reduction (red dashed line). (b) Close examination of the profile near wall. Here, we use D=42 mm, ρ_s=2532.4 kg/m^3, μ=241.8 cP and ρ=1245 kg/m^3

In the second set of comparison, the wall was introduced to a much closer distance at H=1D, 3D and 5D so that the sphere did not develop its terminal velocity before reaching the wall. Using

the same solid sphere and liquid as that employed in the simulation in Fig. 4, the descent velocity profiles are compared in Fig. 5(a). The initial segment of $U_{3D}(t)$ and $U_{5D}(t)$ closely follow $U_\infty(t)$ as if there was no downstream target wall while $U_{1D}(t)$ becomes slower that the rest profiles shortly after the release-around t=0.01 s as shown in Fig. 5(b)-indicating non-negligible wall effect. If we compare $U_{3D}(t)$ to $U_\infty(t)$ and $0.95U_\infty(t)$ in Fig. 5(c), we detected hydrodynamic coupling between t=0.31935 s and 0.31936 s so that the associated gap and velocity data were extracted to estimate $\delta_c^*=1.145\times10^{-2}$ by replacing $0.95U_T$ with $0.95U_\infty(t)$ in Eq. (13). The approach particle Stokes number was evaluated with the instantaneous $U_\infty(t)$ and we obtained St=30.11 for this release.

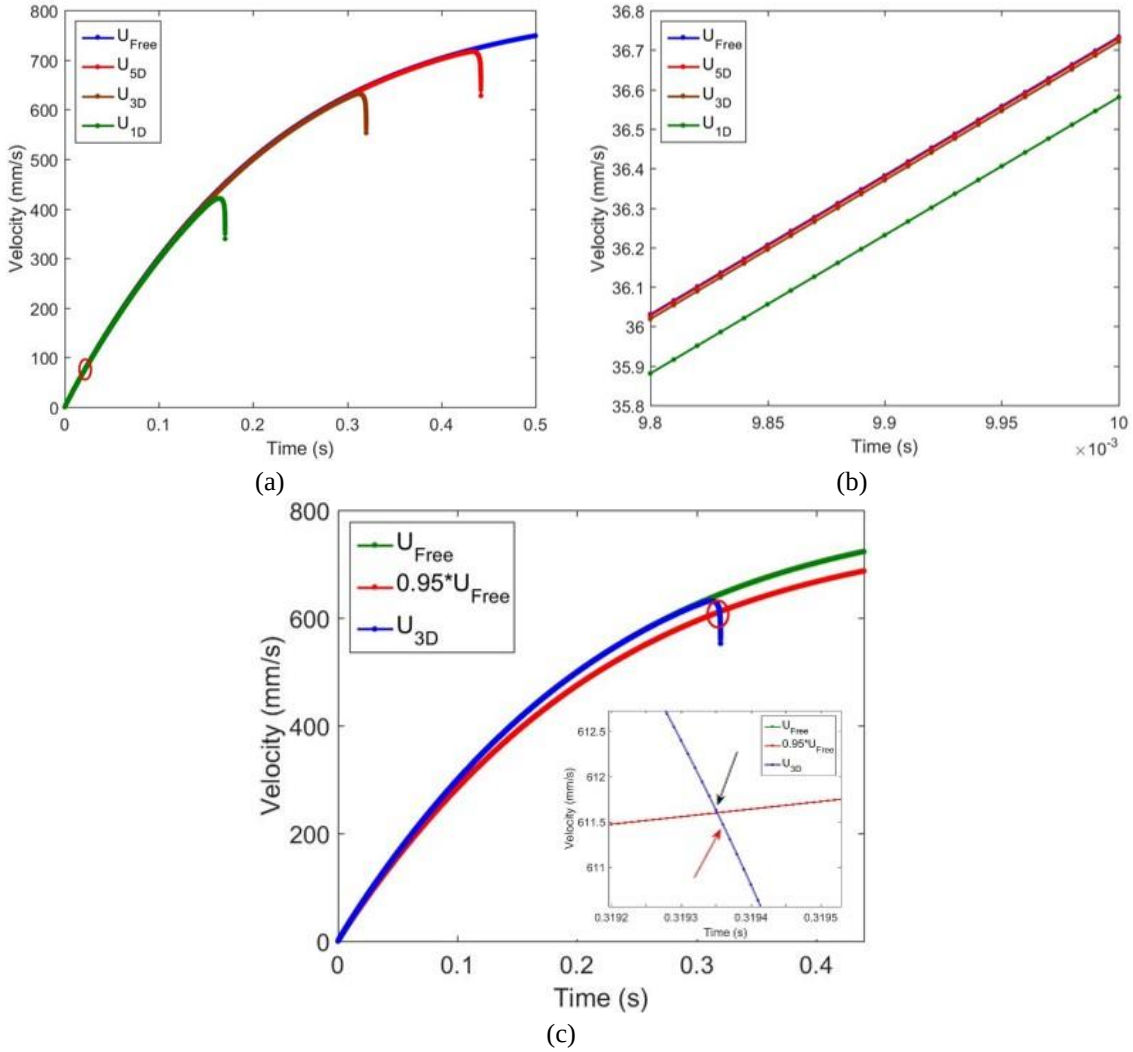

Fig. 5(a) Comparison of the descending velocity profile of a solid sphere released from different heights H=5D, 3D and 1D towards wall to that with no wall (U_{free}). (b) Close examination at early time as that circled in (a). (c) Descent profile from H=3D and its comparison to U_{free} and its 5% reduction in green and red lines, respectively, to extract the occurrence of hydrodynamic coupling Here, we use D=42 mm, ρ_s=2532.4 kg/m^3, μ=241.8 cP and ρ=1245 kg/m^3

By systematically varying μ, H, and two sphere diameters as those summarized in Table 2, we obtained a collection of (δ_c^*, St) for different flow conditions as shown in Fig. 6. We can observe the general trend that the coupling distance decreases monotonically with increasing Stokes number as the particle possessed greater inertia to overcome the wall-amplified hindering hydrodynamic forces. Among these curves, the coupling distance when approaching from constant motion at U_T serves as the lower bound while the release from the smallest H=1D gives an upper envelope. This clearly indicates the significance of the transient hydrodynamic forces and suggests an underestimation of the scaling argument by Izard *et al.* (2014) when only the quasi-steady component is considered. The gradual migration of the δ_c^*-St curves from different drop heights H reveals the significance of particle acceleration on the hydrodynamic coupling phenomenon.

When the sphere has travelled a sufficiently long distance to develop large U towards its terminal velocity, the two unsteady force components F_{AM} and F_H may become comparably negligible to F_{QD} due to both a greater U and smaller dU/dt. Hence, the descents from H>3D will be governed primarily by how a wall modified F_{QD} in Eq. (12) and shall be related to the same near-field correction $C(Re, \delta^*)$ in Eq. (3). For a release from H<3D, the sphere is still in its early acceleration with small U when it moves to the vicinity of the wall and hence the two hindering F_{AM} and F_H should be considered in the equation of motion in addition to F_{QD}. As more terms in Eq. (12) are subject to wall modification, apparent sphere velocity reduction would be detected at a shorter travelled distance to give a greater hydrodynamic coupling distance δ_c^*.

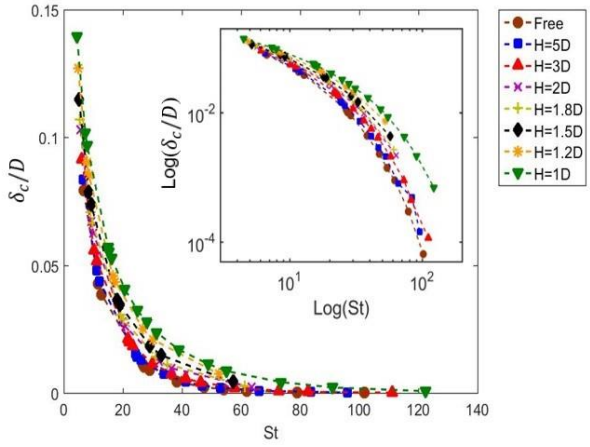

Fig. 6 Coupling distance, scaled by D, to the approach Stokes number for releases from different heights (marked as the multiples of D in the legend) and that approach at terminal velocity (the free case in the legend). The inset presents the data at the logarithmic scale. Note that the coupling distance δ_c is scaled by D here for the same scaling with the release height

Table 2 Summary of the problem parameters used to generate data in Figs. 6 and 7

Sphere	Fluid
Diameter D (mm) =16, 25, 34, 42 Release height $H(D)$=1, 1.2, 1.5, 1.8, 2, 3, 5; 40-80 for the cases reaching U_T Density ρ_s (kg/m^3) =2532.4	Viscosity μ (cP) =46.8 to 241.8 cP Density ρ (kg/m^3) =1245

If we compare the calculated δ_c^*-*St* relation to the prediction by Izard *et al.* (2014) that $\delta_c^* \sim St^{-1}$ in Fig. 7, fair agreement is found only below a threshold *St* above which a much faster decay is discovered. Such a deviation at *St* above a threshold value is the same as what we remark for the experimental data by Joseph *et al.* (2001) in Fig. 1(b) and the threshold *St* is found to be around 30-40 for their data. From our data, the threshold *St* seems to decays with the drop height: around *St*=20-30 for *H*=1*D* but drops to below *St*=10 for the limiting case when approaching at the terminal velocity (marked as 'Free' case).

To provide a quantitative description with the following composite formula

$$\delta_c^* = ASt^{-B}e^{-CSt}. \tag{14}$$

As the δ_c^*-*St* trend varies with the release height *H*, we embed the height-dependence in these coefficients and hence least-square fitting was performed to each group of data from the same *H*. The fitted coefficients are summarized in Table 2 and the variation with *H* are shown in Fig. 8. All the three coefficients decrease with *H* and may be described by the following least-square fitting relations

$$Y(H) = \sigma_1 + \frac{\sigma_2 H}{\sigma_3 + H}, \tag{15}$$

Here, *Y*=*A*, *B* or *C* and σ_i (*i*=1-3) are fitting constants. Clearly, the coefficients *B* is never unity unlike the simple scaling argument by Izard *et al.* (2014) and a refined model will be pursued in the future to take into account of the unsteady hydrodynamic force components.

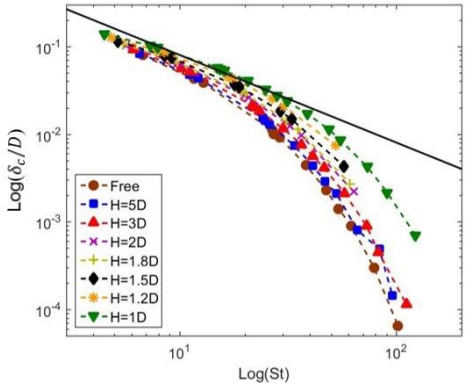

Fig. 7 Comparison of the current δ_c^*-*St* data to the simple scaling argument by Izard *et al.* (2014) as shown by the two solid lines with the slope of -1. Note that the coupling distance δ_c is scaled by *D* here for the same scaling with the release height

Table 3 The value of coefficient *A*, *B* and *C* at different release height *H*

H=	∞	5	3	2	1.8	1.5	1.2	1
A	0.358	0.347	0.340	0.329	0.324	0.323	0.322	0.323
B	0.578	0.567	0.556	0.523	0.508	0.496	0.477	0.461
C	0.060	0.055	0.050	0.046	0.044	0.041	0.037	0.033

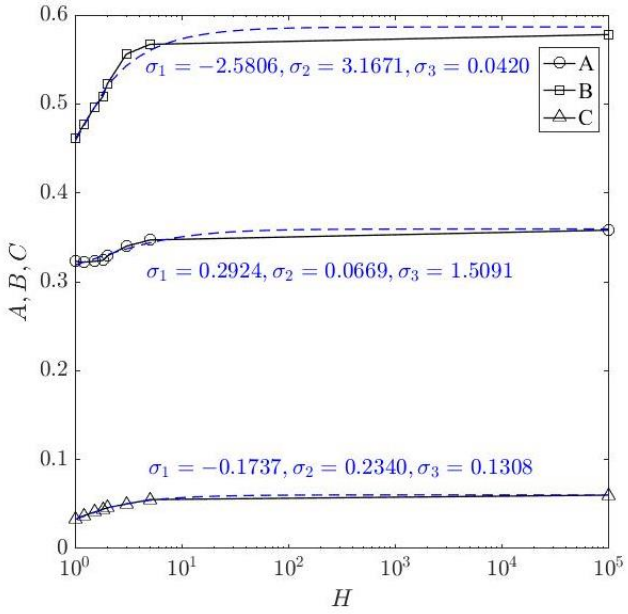

Fig. 8 The variation of fitted coefficients *A*, *B* and *C* with *H*. The blue dash lines denote the least-square fitting relations of Eq. (15)

3. Conclusions

In this work, we study the phenomenon of hydrodynamic coupling using the dynamics of a fully-immersed solid sphere in vertical descent towards a horizontal wall predicted by a hydrodynamic model. This model incorporates both wall augmentation effect on the quasi-steady viscous force F_{QD}, the added mass force F_{AM}, and the history force F_H as well as the modification on F_{QD} and F_H due to liquid inertia. The interstitial gap when the near-wall approach velocity dropped 5% from the velocity developed as if there was no downstream wall was used to determine a hydrodynamic coupling distance δ_c. The associated no-wall approach velocity is used to estimate an approach Stokes number, *St*, and used to study how δ_c varies with *St*. By systematically changing the sphere size, release height, and liquid viscosity, we achieve sphere approaches both at its terminal velocity and in acceleration over $6<St<120$. A general trend is discovered that the diameter-scaled coupling distance, $\delta_c^* = \delta_c / D$, diminishes monotonically with local *St* but at a rate faster than the literature scaling relation $\delta_c^* \sim St^{-1}$ above a threshold value from $St=10$ to 40. Furthermore, the δ_c^*-*St* relation shows dependence on the drop height to migrate gradually from the lower bound with a constant approach at the terminal velocity to an upper bound from the smallest drop height. This clearly indicates that the two unsteady force components F_{AM} and F_H should not be left out in developing a model for δ_c^* and an additional dimensionless parameter that measures the effect of particle acceleration may be useful. As a first attempt towards a practical model, we attempt a fitting relation that $\delta_c^*(St, H^*)=A(H^*)St^{-B(H^*)}e^{-C(H^*)St}$ embedding the particle acceleration effect in the dependence of fitting constants on the diameter-scaled drop height.

4. Discussions

Other than developing a refined model for $\delta_c^*(St, H^*)$, there are a few other issues remain to be further investigated. The first is how the correction factor $C(Re, \delta^*)$ on the quasi-steady viscous drag should be switched between a far-field and a near-field correction. The other issue is how the history force is modified for the downstream wall as the current factor is developed from the boundary layer theory which does not apply in the creeping flow regime. It will require accurate numerical simulation or careful experimental measurement to clarify the liquid inertial effect on the analytic correction factor in Eq. (3) and the $H(\delta^*)$ factor in Eq. (8).

Acknowledgments

This project was supported by the Ministry of Science and Technology of Taiwan through Grants No. 105-2221-E-002-101 and No. 106-2628-E-002-012-MY3.

References

Clift, R., Grace, J.R. and Weber, M.E. (1978), *Bubbles, Drops, and Particles*, Academic Press, New York, U.S.A.

Cox, R.G. and Brenner, H. (1967), "The slow motion of a sphere through a viscous fluid towards a plane surface-II small gap widths, including inertial effects", *Chem. Eng. Sci.*, **22**(12), 1753-1777.

Davis, R.H., Serayssol, J.M. and Hinch, E.J. (1986), "The elastohydrodynamic collision of two spheres", *J. Flu. Mech.*, **163**, 479-497.

Gondret, P., Lance, M. and Petit, L. (2002), "Bouncing motion of spherical particles in fluids", *Phys. Flu.* **14**(2), 643-652.

Hou, G., Wang, J. and Layton, A. (2012), "Numerical methods for fluid-structure interaction-a review", *Commun. Comput. Phys.*, **12**(2), 337-377.

Ibrahimbegovic, A., Kassiotis, C. and Niekamp, R. (2016), "Fluid-structure interaction problems solution by operator split methods and efficient software development by code-coupling", *Coupled Syst. Mech.*, **5**(2), 145-156.

Izard, E., Bonometti, T. and Lacaze, L. (2014), "Modelling the dynamics of a sphere approaching and bouncing on a wall in a viscous fluid", *J. Flu. Mech.*, **747**, 422-446.

Joseph, G.G., Zenit, R., Hunt, M.L. and Rosenwinkel, A.M. (2001), "Particle wall collisions in a viscous fluid", *J. Flu. Mech.*, **433**, 329-346.

Kempe, T. and Fröhlich, J. (2012), "Collision modelling for the interface-resolved simulation of spherical particles in viscous fluids", *J. Flu. Mech.*, **709**, 445-489.

Lefrançois, E., Brandely, A. and Mottelet, S. (2016), "Strongly coupling partitioned scheme for enhanced added mass computation in 2D fluid-structure interaction", *Coupled Syst. Mech.*, **5**(3), 235-254.

Li, X., Hunt, M.L, and Colonius, T. (2011), "A contact model for normal immersed collisions between a particle and a wall", *J. Flu. Mech.*, **691**, 123-145.

Mei, R. and Adrian, R.J. (1992), "Flow past a sphere with an oscillation in the free-stream velocity and unsteady drag at finite Reynolds number", *J. Flu. Mech.*, **237**, 323-341.

Simeonov, J.A. (2015), "The unsteady hydrodynamic force during the collision of two spheres in a viscous fluid", *Acta Mech.*, **227**(2), 565-580.

Soares Jr, D. (2012), "FEM-BEM iterative coupling procedures to analyze interacting wave propagation models: Fluid-fluid, solid-solid and fluid-solid analyses", *Coupled Syst. Mech.*, **1**(1), 19-37.

Le Tallec, P. and Mouro, J. (2001), "Fluid structure interaction with large structural displacements",

Comput. Meth. Appl. Mech. Eng., **190**(24-25), 3039-3067.
Wang, C. and Eldredge, J.D. (2015), "Strongly coupled dynamics of fluids and rigid-body systems with the immersed boundary projection method", *J. Comput. Phys.*, **295**, 87-113.
Yang F.L. (2006), "Interaction law for a collision between two solid particles in a viscous liquid", Ph.D. Dissertation, California Institute of Technology, California, U.S.A.
Yang, F.L. (2010), "A formula for the wall-amplified added mass coefficient for a solid sphere in normal approach to a wall and its application for such motion at low Reynolds number", *Phys. Flu.*, **22**(12), 123303.
Yang, F.L. and Hunt, M.L. (2006), "Dynamics of particle-particle collisions in a viscous liquid", *Phys. Flu.*, **18**(12), 121506.

DC